Analytical Methods for Upscaling of Fractured Geological Reservoirs

Pål Næverlid Sævik

Dissertation for the degree of Philosophiae Doctor (PhD)

Department of Mathematics
University of Bergen

May 2015

Dissertation date: 16. oktober, 2015

Preface

This dissertation is submitted as a partial fulfillment of the requirements for the degree Doctor Philosophy (PhD) at the University of Bergen. The advisory committee has consisted of *Inga Berre* (Department of Mathematics, University of Bergen), *Martha Økland Lien* (Uni Research CIPR, University of Bergen and Octio AS), and *Morten Jakobsen* (Department of Earth Science, University of Bergen).

The PhD project has been financially supported by Statoil ASA through the Akademia agreement.

Abstract

Numerical simulations have become an essential tool for planning well operations in the subsurface, whether the application is petroleum production, geothermal energy, groundwater utilization or waste disposal and leakage. To represent a complicated heterogeneous subsurface reservoir in a simulator model, material properties within each part of the reservoir are replaced by *effective* properties through upscaling. In this thesis, analytical upscaling methods for fractured reservoirs are studied, with special emphasis on *effective medium methods*. These methods have been suggested for fracture upscaling by a number of authors, but reliable analytical error estimates and comparisons with comprehensive numerical simulations have been lacking.

The work in this thesis evaluates the accuracy of effective medium methods by providing an extensive comparison between analytical and numerical estimates, for both isotropic and anisotropic three-dimensional fracture configurations. The estimates are also analyzed with respect to known theoretical results, such as rigorous upper and lower bounds, asymptotic behavior and percolation properties.

It is found that one of the effective medium variants, the asymmetric self-consistent method, has the correct asymptotic behavior, satisfy all analytical bounds, and agree well with numerical percolation results. This is somewhat surprising, since the method has been regarded in the literature as having the weakest theoretical foundation. One explanation for the good results may be the special geometry that a fracture/matrix system represents, which agree well with the way the method is defined and derived.

As a part of the work in this thesis, effective medium formulations that are numerically stable for arbitrarily thin inclusions are developed. The formulations show good convergence properties in the general anisotropic case, and explicit expressions for the isotropic and slightly anisotropic case are also given. In the case of very thin inclusions, the new formulations allows the number of input parameters to be reduced.

Finally, the thesis investigates the use of assisted history matching for fractured reservoirs. It is shown that history matching of upscaled models may generate parameter distributions that are inconsistent with the underlying fracture description, resulting in unphysical connectivity estimates for the fracture network. The problem can be avoided by history matching the fracture parameters directly, and include fracture upscaling as an integral part of the parameter inversion framework. This adds to the computational cost, but the additional computational effort is negligible if analytical fracture upscaling is used.

Outline

This thesis is organized into two parts. The first part gives an overview of scientific theory and mathematical methods that are relevant to the thesis. The second part contains papers that are either published or submitted for publication in scientific journals.

Part I is structured into six main chapters as follows:

Chapter 1 motivates the use of analytical upscaling methods for fractured geological reservoirs, and summarizes the main contributions of the thesis.

Chapter 2 presents common parameters used to characterize fractured reservoirs, and how they are measured in the field.

Chapter 3 describes the standard equations used to model flow in fractured porous media. Since some of the included papers also deal with electrical conductivity, a short overview of the equations governing flow of electrical currents is given as well.

Chapter 4 gives the definition of effective permeability and conductivity and introduces some basic upscaling methods for estimating these quantities.

Chapter 5 provides a short introduction to ensemble-based parameter inversion, which is relevant to the issues discussed in Paper D.

Chapter 6 gives an overview of all the included papers and their scientific contributions.

Part II contains the following scientific papers:

Paper A Sævik, P. N., Berre, I., Jakobsen, M., and Lien, M. Electrical conductivity of fractured media: A computational study of the self-consistent method. *In SEG Technical Program Expanded Abstracts* (2012). Society of Exploration Geophysicists. doi: 10.1190/segam2012-1026.1

Paper B Sævik, P. N., Berre, I., Jakobsen, M., and Lien, M. A 3D Computational Study of Effective Medium Methods Applied to Fractured Media. *Transport in Porous Media 100*, 1 (2013), 115–142. doi: 10.1007/s11242-013-0208-0

Paper C Sævik, P. N., Jakobsen, M., Lien, M., and Berre, I. Anisotropic effective conductivity in fractured rocks by explicit effective medium methods. *Geophysical Prospecting 62*, 6 (2014), 1297–1314. doi: 10.1111/1365-2478.12173

Paper D Sævik, P. N., Lien, M., and Berre, I. An integrated approach to upscaling and history matching of fractured reservoirs. *Submitted to Water Resources Research* (2015).

Acknowledgments

I have been fortunate to have Inga Berre, Martha Økland Lien and Morten Jakobsen as supervisors during my time as a PhD student. Through lively discussions and insightful suggestions, they have all provided valuable guidance for my research, each in their own unique way.

I am very grateful for my friends and colleagues at the Department of Mathematics and Uni CIPR, both for the rewarding scientific environment they provide, and for the welcoming and light-hearted atmosphere that characterizes our working environment. A special thanks goes to Svenn and Kristian for all the coffee-breaks and enriching discussions we have had throughout the years. I thank Margot Gerritsen for hosting me at Stanford University for five months, which helped me broaden my perspectives on reservoir simulation and uncertainty quantification.

I am indebted to my parents Margaret and Inge for stimulating my curiosity and encouraging me to pursue a scientific career, and for always keeping me in their thoughts and prayers.

Finally, the biggest thanks goes to my wife Elisabeth and our sweet boys Daniel and Filip, without whom the writing of this thesis would be so much less fullfilling.

Contents

Part I

Scientific background

Chapter 1

Introduction

The study of fluid flow in underground geological structures has relevance to widely different applications, including petroleum production, utilization of geothermal energy, groundwater management and underground contamination assessment. In all of these applications, mathematical and numerical modeling plays an important role. Numerical computer simulations can be used to predict the outcome of a given drilling and production strategy, and assess the financial and environmental risks associated with possible scenarios. Mathematical tools are also used to infer physical properties of an underground reservoir, which are difficult to obtain by direct measurements.

Rocks may be permeable to fluid flow due to the microscopic pore space between the rock grains, and/or due to fractures and larger cavities (vugs) within the rock. Fractures may form as a result of natural processes, such as faulting and folding, or they may be engineered for enhanced reservoir permeability. Petroleum producing wells are often hydraulically fractured as a routine part of their completion [34], and the production of oil and gas from tight shale formations depend entirely on the ability to create fractures within the formation by hydraulic stimulation. In geothermal reservoirs, reservoir permeability can be improved by hydraulically induced fracture shearing, which enhances the permeability of the existing natural fracture networks [27].

Mathematical modeling of flow and transport in a fractured reservoir is challenging for a number of reasons. First of all, the macroscopic material properties of fractured rock is difficult to measure directly, since core samples taken during well drilling are much smaller than the typical fracture size. Secondly, fractured reservoirs often have anisotropic characteristics, due to the fact that fractures often form along certain preferential directions. Third, fractured reservoirs may exhibit dual porosity behavior, where the fractures and the surrounding rock matrix behave as two separate, interacting media. A fourth complication is that large fractures often need to be modeled explicitly, since the preferential pathways they create are difficult to capture in a standard grid-block numerical model.

Because of the computational cost, it is infeasible to represent all fractures explicitly in a numerical model. A more viable strategy is to use a *continuum model* for the small scale fractures. In a continuum formulation, the fractured rock is modeled as an unfractured, homogeneous medium with modified material properties, correspond-

ing to the *effective* (macroscopic) properties of the fractured rock. These properties may be estimated using upscaling techniques, where statistical information on fracture density, orientation, size etc. are used as input parameters. Upscaling techniques can also be used the other way around, by establishing bounds on the fracture parameters based on certain macroscopic measurements. For instance, information from seismic surveys can be used to infer some of the fracture properties, which in turn can be used to limit the feasible range of effective hydraulic permeability.

Fracture upscaling can be performed by analytical or numerical methods. In numerical upscaling, a geometric representation of the fracture network is generated and meshed. A set of boundary conditions is applied, and the resulting flux through the matrix-fracture system is calculated. This approach is accurate if the true fracture geometry is known, the boundary conditions conform to the flow directions in the field, and a fine mesh is generated for the fracture network. On the other hand, accurate numerical upscaling is computationally demanding.

In analytical upscaling, the true fracture network is represented by a simplified, idealized geometry, whose properties is calculated analytically. Analytical methods are fast, but may not always be applicable. In particular, they require that the fractured rock is *macroscopically homogeneous*, which is implies that no large-scale features are permitted within the upscaling domain.

A particular class of analytical upscaling methods given much attention in this thesis, are the methods based on *effective medium theory*. This framework for upscaling of heterogeneous materials has a long history, starting with the works of Maxwell [45], Bruggeman [9] and Eshelby [19]. By theoretical considerations, effective medium theory is expected to give accurate estimates for homogeneous materials containing well-separated, rounded inclusions. A particular effective medium method known as the *symmetric self-consistent method* is also known to be a good approximation for materials that possess phase symmetry, such as polycrystals [68].

The use of effective medium theory for estimating the hydraulic permeability and electrical conductivity of fractured rocks has been suggested by a number of authors [5, 7, 23, 56]. Nevertheless, the quality of these estimates for dense fracture networks has been questioned, partly due to the lack of reliable error estimates [31, 68]. In the included Paper A and B, this objection is addressed by applying three commonly used effective medium methods to a variety of fracture configurations, and comparing the estimates with results from numerical upscaling. In addition, the methods are compared with the alternative analytical upscaling approach of Mourzenko et al [50].

Paper A and B also address a problem with traditional effective medium formulas, which is that they become numerically unstable for inclusions of vanishing thickness. To overcome this limitation, the papers present a novel set of formulas that are numerically stable for arbitrarily thin inclusions. The new formulas show fast and reliable convergence behavior for isotropic and anisotropic media, below and above the percolation threshold, for all levels of matrix/fracture conductivity contrast. They also require a smaller number of input variables, compared with the traditional formulation.

The effective medium methods presented in Paper A and B are *implicit* formu-

lations, which must be solved by iterative algorithms. In a similar manner, Paper C is concerned with *explicit* effective medium methods. The benefits of explicit methods are ease of use, computational efficiency and the ability of computing analytical derivatives. On the other hand, the methods are not applicable to media that are both strongly heterogeneous and strongly anisotropic.

Similar to Paper A and B, Paper C presents novel formulas for existing explicit effective medium methods, that are numerically stable for inclusions of vanishing thickness. Furthermore, three novel explicit schemes for anisotropic media are constructed, based on an implicit scheme previously suggested by Berryman and Hoversten [7]. The methods in the paper are applied to various fracture configurations, and the estimates are compared with results from numerical upscaling.

In Paper D, a different issue regarding analytical fracture upscaling is addressed. Upscaled models of fractured reservoirs are commonly calibrated (or *history matched*) to measured well data, to improve the predictive quality of the model. However, the calibration is commonly performed on upscaled parameters instead of fracture parameters. Paper D shows that this approach may give upscaled variables that are inconsistent with the underlying fracture model, and may also result in a larger mismatch between measured and predicted data. Improved results with internally consistent variables are obtained when fracture parameters are calibrated directly, and fracture upscaling is included as an integral part of the history matching workflow. Although this has an added computational cost, the difference is negligible if analytical upscaling methods are used.

Chapter 2

Characterization of fractured reservoirs

From a geomechanical point of view, a *fracture* is a part of the rock where tensile and shear stress has caused partial loss of cohesion. Due to the mechanisms responsible for crack and fracture generation, fractures are usually planar or near-planar, with a thickness much smaller than their lateral extent. The *matrix* is the rock surrounding the fractures, including the pore space within the rock[1]. Usually, the pore throats within the rock matrix are small compared to the thickness of the fractures. Because of this, fractures provide a high-permeable pathway for fluid flow through the rock, unless they have been sealed over time due to mineral depositions. They may also provide a preferential conduit for electrical currents if they are filled with a highly conductive fluid or mineral.

Fractured reservoirs can be described, or *characterized*, in a number of different ways. In this chapter, we focus on the geometrical properties of the fracture network, and the parameters commonly used to describe them. Geological, geophysical and hydraulic investigations can reveal fracture information on different scales, from micrometer-scale investigations of the interior fracture geometry to macroscopic surveys determining the connectivity of the fracture network.

Common techniques used to obtain fracture parameters are laboratory studies of wellbore core samples, field studies of outcrop analogs, seismic and electromagnetic surveys, different variants of well logging, hydraulic well testing and tracer injection tests [28, 64]. Information on likely fracture parameter values can also be inferred from the lithology and stress field within the reservoir. In core sample studies and outcrop studies, fracture parameters are measured directly, whereas the other methods mentioned above are indirect measurement techniques based on the macroscopic physical behavior of fractured media. The coupling between fracture parameters and macroscopic properties are discussed in more detail in Chapter 4.

[1] In non-fractured reservoirs, the term «matrix» is often used to describe the rock phase itself, excluding the pore space between the rock grains.

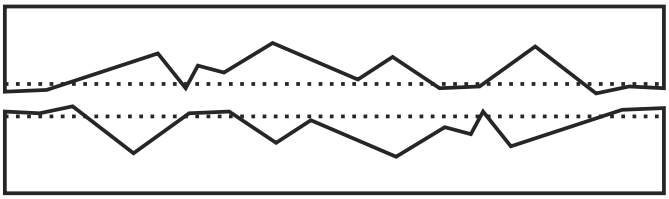

Figure 2.1: Rough-walled fracture. The hydraulic aperture is indicated by dashed lines.

2.1 Characterization of the fracture interior

Although it is mathematically convenient to model a fracture as a two-dimensional feature, fractures have a complex three-dimensional interior geometry, which must be taken into account during fracture characterization. Interior fracture properties may vary greatly, depending on the stresses responsible for creating the fracture, the properties of the rock, and the physical processes taking place inside the fracture after its formation. To determine the interior properties of fractures in a specific reservoir, laboratory studies of core samples can be helpful, as well as studies of outcrop analogs. Some information may also be obtained from geological interpretation, by considering typical fracture characteristics for the lithology and stress field within the formation.

2.1.1 Aperture

Of the most important fracture characteristics is the fracture aperture, which is the distance between the fracture walls. Commonly, fractures in subsurface rocks have small apertures due to overburden stress [64]. Tensile fractures, which are typically created due to folding processes, tend to have larger apertures than shear fractures, which form in response to shear stresses. Over time, the fracture aperture may increase or decrease due to mineral dissolution or precipitation reactions.

For a rough-walled fracture, a distinction is often made between the *mechanical aperture* and *hydraulic aperture*. The mechanical aperture is the true, physical distance between the fracture walls, sometimes defined as an average over the whole fracture. The definition of the hydraulic aperture, on the other hand, is based on how easily a fluid can flow through the fracture. Specifically, the flow rate through a fracture with hydraulic aperture a is equal to the flow rate through a hypothetical smooth-walled fracture with mechanical aperture a, when subject to the same boundary conditions [58]. In practice, the hydraulic aperture is always smaller than the mechanical aperture, due to the additional friction created by fracture wall roughness. A simple illustration is given in Figure 2.1.

2.1.2 Roughness

The roughness of a fracture can potentially be defined as a geometric quantity, e.g., as the mean height of the fracture irregularities divided by the mean mechanical aperture [64]. From a hydrodynamical point of view, it is often more convenient to define

roughness as the ratio of mechanical to hydraulic aperture. For this definition to be well-defined, the flow within the fracture must be laminar, otherwise the value of the hydraulic aperture would depend on the fluid velocity. An indication of whether or not the flow is laminar, is given by the Reynolds number,

$$\mathrm{Re} = \frac{\rho V D_h}{\mu}, \tag{2.1}$$

where ρ is the fluid mass density, μ is the fluid viscosity, V is the velocity of the fluid, and D_h is the hydraulic diameter, defined as

$$D_h = 4A/P, \tag{2.2}$$

where A is the cross-sectional area of the fracture, and P is the perimeter of the cross section [16]. Experimental data indicate that the transition from laminar to turbulent flow occurs at Reynolds numbers between 100 and 2300, depending on the fracture roughness [43, 64].

In the included papers, it is consistently assumed that the flow within the fractures is laminar. In practice, this assumption may be violated near production and injection wells, where fractures are wide and the fluid velocity is high.

2.1.3 Filler material

Not all fractures have an open space between the fracture walls. The walls of a fracture may be heavily coated by precipitated minerals, or the entire pore space may be filled with mineral deposits. In this case, flow within the fracture is subject to the same physical laws as the surrounding porous rock, only with different material properties, which may be measured by laboratory studies. Mineral deposits may preserve or destroy fracture permeability, depending on the deposition process [42].

Porous rocks may contain low-permeable, planar features that are usually not classified as fractures since they are generated by different processes. For instance, deformation bands, dykes and stylolites fall into this category [24, 28, 30]. Although different in origin, these structures can be treated as cemented fractures from a hydraulic point of view. They may be characterized using laboratory measurements and general geological interpretation.

2.2 Characterization of individual fractures

It is difficult to make direct measurements of the geometry of individual fractures, since a fracture is typically much larger than the size of a core sample, and smaller than the resolution of seismic imaging techniques. Furthermore, tight fractures that do not cause shearing may not show up on seismic images regardless of their size. To gain information on the size, shape and orientation of fractures, one may instead take advantage of indirect measurements from well logs, and anomalies detected during seismic or electromagnetic surveys [28, 64]. Outcrop analogs may also provide a valuable source of information, as well as general knowledge on typical parameter values based on geological interpretation of lithology and formation stress.

2.2.1 Size

The fracture length, or persistence, is a major factor controlling the connectivity of the fracture network. Fractures that are much longer than the typical fracture spacing tend to form a well-connected network, and fractures much smaller than the typical spacing tend to be isolated. The fracture length is a difficult parameter to quantify, and the best source of information may be outcrop analogs. When recording the length of exposed fractures in the outcrop, one should take care to correct for various types of biases such as the inability to measure the full fracture length due to incomplete exposures [14].

Natural fractures are polydisperse, meaning that fractures of different size occur within the same reservoir volume. The power law distribution is commonly used to describe the statistical variation of fracture sizes [8].

2.2.2 Shape

All real fractures are irregular, but in both analytical and numerical models the fracture shape is usually approximated by an idealized geometrical shape, such as a hexagon or an ellipsoid. Virtually all synthetic fracture models assume that the fractures are planar, although natural fractures may be bent and curved to some degree. Elongated fractures may cause anisotropy in the direction of the elongation, and the degree of elongation may be included in the fracture model. Furthermore, the choice of a representative fracture shape may affect the estimated connectivity of the network [50].

2.2.3 Orientation

Fracture orientation is commonly described by the parameters *dip* and *strike* [29]. The strike refers to the direction of the horizontal tangent vector, which is found by intersecting the fracture with a horizontal plane. The dip angle is the angle between the fracture and the horizontal plane. Sometimes the parameter *dip direction* is used instead of the strike, defined as the direction orthogonal to the strike and tangential to the fracture, pointing downwards. Yet another way of describing orientation is by giving the coordinates of the *unit normal vector* (or *pole*), which points in the direction orthogonal to the fracture plane. The different ways of describing fracture orientation is illustrated in Figure 2.2.

Due to the stress field and the geological history of a fractured rock, natural fractures often show a preferential orientation in one or several directions. For this reason, fractures are often divided into *sets* (or *families*), each with separate main directions. A statistical distribution, such as the Fisher distribution [21, 51], is then used to describe the fracture orientations within each set.

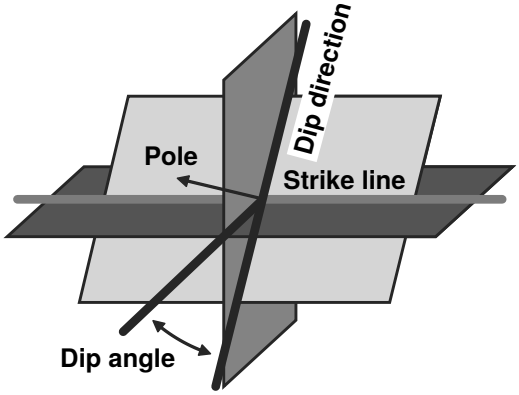

Figure 2.2: Terminology for fracture orientation

2.3 Characterization of a fracture network

The effective properties of a fracture network are not only dependent on the mean properties of fractures constituting the network, but also on the geometry of the network as a whole. The fracture network can be characterized by a number of geometrical and topological parameters, with fracture density and connectivity being the most important ones. These parameters can be found by outcrop studies and wellbore samples, as well as indirect measurements such as tracer tests.

2.3.1 Fracture density

Fracture density, also called *fracture intensity*, describes the amount of fractures present in the reservoir. Dershowitz and Herda [17] identified 6 ways of defining fracture density, based on the measured quantity (i.e., fracture length, spacing, surface area, volume or number of fractures), and the dimension of the measurement region (i.e., lineal, areal or volumetric). In three-dimensional fracture models, the most useful measure is arguably the fracture surface area per volume (the *P32 density*), and its dimensionless variant which is the P32 density scaled by the fracture size.

Balberg et al. [4] showed that the dimensionless P32 density is directly proportional to the average number of intersections per fracture. Thus, the measure is directly related to the connectivity of the fracture network. Furthermore, Mourzenko et al. [49] showed that the effective permeability of a fracture network is almost insensitive to the fracture size distribution, if the dimensionless P32 fracture density is fixed. It is therefore more important to know the fracture density of the system than having detailed knowledge on the variation in fracture sizes.

2.3.2 Fracture connectivity

The connectivity of a fracture network can be characterized in many ways [59], using topological parameters (e.g., Betti numbers, Euler characteristics, coordination num-

bers), geometrical parameters (e.g., tortuosity, fraction of isolated fractures, cluster sizes) or by hydraulic parameters (e.g., true fracture network permeability vs. permeability in a fully connected network). In the included papers, the latter approach is used. Specifically, connectivity is defined as a parameter between 0 and 1, where 0 represents a disconnected set of fractures that does not contribute to permeability, and 1 corresponds to the fully connected case which gives the maximal permeability contribution.

If the fractures have a polygonal or circular shape of fixed size, are randomly distributed in space, and the fractured domain is infinitely large, then the connectivity of the fracture network is only a function of the dimensionless P32 fracture density [68, 75]. If the fracture density drops below a critical value (the *percolation threshold*), the network becomes unconnected, meaning that there are no clusters of connected fractures that are infinitely large. Just above the critical density, the effective permeability of the fracture network is proportional to $(\rho - \rho_c)^2$, where ρ is the dimensionless P32 fracture density, and ρ_c is the percolation threshold [50, 68].

In a domain of finite size, the percolation threshold is defined as the density where there is a 50% chance of the network being connected. The effect of the domain size on percolation properties has been studied by Mourzenko et al [49]. Their results show that the percolation thresholds for finite and infinite domains are similar when the size of the domain is an order of magnitude larger than the fracture size, and the fractures are randomly oriented.

2.3.3 Matrix connectivity

If the fractures act as barriers to flow due to cementation, the connectivity of the fracture network itself is of less importance. Instead, the connectivity of the surrounding rock matrix becomes a crucial factor. For randomly distributed fractures with a fixed size and shape within an infinite domain, the matrix is connected only if the fracture density is smaller than the *void percolation threshold* [76]. If the rock matrix is connected, fluid flowing through the domain can bypass the fractures by going through the matrix, and the impact of the fractures is small. On the other hand, if cemented fractures divide the rock matrix into isolated regions, the fluid must go through the fractures as well. This results in a significantly smaller effective permeability of the rock.

Chapter 3

Mathematical framework

At the heart of any reservoir simulation tool lies the mathematical equations used to describe the simulated physical processes. In this chapter, a short introduction to the standard equations describing single- and multiphase fluid flow in porous rocks is given. The multiphase situation is particularly interesting when the rock is fractured, since capillary forces may play a dominant role in this case. We also introduce the dual-continuum formulation, which is often used to separate flow in the fractures and the surrounding rock matrix.

In the last part of the chapter, a brief description of Maxwell's equations is given, which are used to model electromagnetic processes within the reservoir. Electromagnetic techniques are important tools in reservoir characterization, and may also be used to estimate some of the fracture parameters described in Chapter 2.

3.1 Single-phase flow in porous media

A rock may be permeable to fluid flow due to the microscopic pore space between the rock grains, and/or due to fractures and larger cavities (vugs) within the rock. At the microscopic level, fluid flow within the pores and fractures of a rock is accurately described by the Navier-Stokes equations. Solving these equations is computationally demanding even for small rock samples, and requires detailed knowledge on the pore geometry within the rock. On the reservoir scale, one is not interested in the fluid movement within each individual rock pore, but rather in the bulk movement of the fluid, called the *volume flux*. Fortunately, the volume flux can be described by equations that are computationally much more tractable than the Navier-Stokes equations.

3.1.1 Darcy's law

In a porous medium, the volume flux is related to the fluid pressure through *Darcy's law*, which was first found empirically by the french engineer Henry Darcy [64]. Later, it has been shown to be consistent with the Navier-Stokes equations under certain assumptions that are usually satisfied for flow in porous rocks [73]. Using common

notation, Darcy's law is expressed as

$$\mathbf{u} = -\frac{\mathbf{K}}{\mu}(\nabla p - \rho g \nabla z) \tag{3.1}$$

where $\mathbf{u}$ is the volume flux (sometimes called the *Darcy velocity*), $\mathbf{K}$ is the tensor-valued hydraulic permeability of the rock, μ is the fluid viscosity, p is the fluid pressure, ρ is the fluid mass density, g is the acceleration of gravity, and z is the coordinate for the vertical direction.

3.1.2 Fluid properties

Darcy's law contains two parameters that are properties of the fluid within the pore space of the rock, namely the fluid mass density ρ and the fluid viscosity μ. Both of these properties are generally state variables, thus they may be functions of on the fluid pressure and temperature. Whether or not this dependence is of importance, is determined by the specific application. For instance, the viscosity often changes with temperature, but not so much with pressure, and may be regarded as constant in isothermal reservoirs. The mass density of water in the liquid state is largely insensitive to moderate changes in pressure and temperature, and is often taken to be constant as well. On the other hand, the density of liquid oil may be much more likely to change significantly with pressure and temperature.

3.1.3 Rock permeability

The rock permeability $\mathbf{K}$ is a positive definite tensor, and it is usually assumed to be symmetric. The value of the permeability is directly related to the pore geometry within the rock, most notably the density, size and tortuosity of the pores. In practice, the permeability is usually determined from laboratory experiments on core samples taken during drilling, and from analysis of transient pressure behavior during well testing [34].

3.1.4 Fracture permeability

As explained in Section 2.1.3, some fractures may be filled with mineral deposits, and flow within these fractures is physically similar to flow within the porous rock matrix. To find the intrinsic permeability of a cemented fracture, laboratory tests of core samples can be used.

For open fractures, the concept of «fracture permeability» is more complicated. For this concept to make sense, the volume flux through the fracture must be proportional to the applied pressure gradient, at least for small fluid velocities. It can be easily shown from the Navier-Stokes equations that the volume flux through a smooth-walled, infinitely extending fracture is given by the expression

$$\mathbf{u} = -\frac{a^2}{12\mu}(\nabla p - \rho g \nabla z)\,, \tag{3.2}$$

where a is the mechanical fracture aperture, and we have assumed that ∇p points in the tangential direction [77]. This expression is clearly consistent with Darcy's law (3.1), with

$$\mathbf{K} = \frac{a^2}{12}\mathbf{I}. \tag{3.3}$$

Since the effective permeability of the fracture network is proportional to both the intrinsic fracture permeability given by (3.3), and the total porosity (volume fraction) of the fractures, flow through smooth-walled fractures is effectively proportional to the cube of the aperture. This is usually referred to as the *cubic law*.

In a rough-walled fracture, volume flux is not necessarily linearly dependent on the pressure gradient, either because of inertial effects, or because of turbulent flow. As explained in Section 3.3, the dimensionless Reynolds number may be used as an indication of which flow regime is present. In the included papers, it is assumed that the flow velocity is sufficiently small to give a linear relation between volume flux and pressure gradient. In this case, Darcy's law (3.1) may be used to calculate flow both in both the fracture and the matrix. Equation (3.3) represents an upper bound on the intrinsic fracture permeability, while the true permeability can either be measured directly, or estimated from the mechanical aperture and the roughness of the fracture [58].

3.1.5 Mass conservation

In addition to Darcy's law (3.1), the full set of equations describing fluid flow includes the *mass conservation equation*. This equation is derived by observing that the fluid mass change within an arbitrary domain is equal to the mass influx plus the contribution from mass sources (e.g., production and injection wells). Mathematically, this is formulated as

$$\frac{\partial}{\partial t}\iiint_{\Omega} \phi\rho \, d\Omega = -\oiint_{\partial\Omega} \rho\mathbf{u}\cdot\mathbf{n}\, dS + \iiint_{\Omega} q \, d\Omega, \tag{3.4}$$

where ϕ is the fraction of pore volume within the rock (the *porosity*), $\mathbf{n}$ is the outward surface normal, q is a mass source term, and Ω is an arbitrary domain. Applying the divergence theorem, and using the fact that the equation is valid for any domain, we arrive at the local form of the equation,

$$\frac{\partial}{\partial t}(\phi\rho) = -\nabla\cdot(\rho\mathbf{u}) + q. \tag{3.5}$$

3.2 Multiphase flow in porous media

Multiple fluid phases may co-exist within the same rock formation, such as oil, water and gas in petroleum reservoirs, water and steam in geothermal reservoirs, and water and supercritical CO_2 in aquifers used for CO_2 storage. The presence of multiple phases leads to additional physical effects, which must be accounted for in the mathematical models for flow and transport. For instance, capillary pressure may cause a wetting fluid to displace a non-wetting fluid, even without the presence of an external

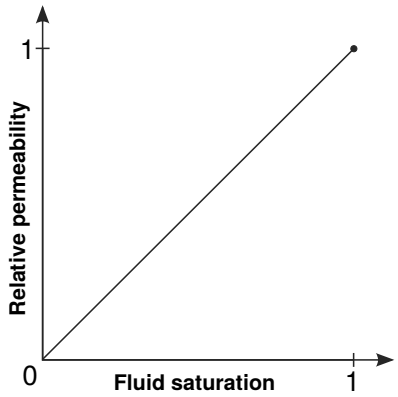

Figure 3.1: Linear relative permeability, which is commonly assumed within fractures.

pressure gradient. Furthermore, phases that co-exist within the same rock volume effectively reduce the permeability of the rock. Common models for these multiphase effects are introduced below.

3.2.1 Relative permeability

In a multiphase system, each fluid phase occupy some of the pore volume, thereby effectively reducing the pore volume available to the other flowing phases. Thus, the volume flux of each fluid phase is reduced accordingly. This physical effect is commonly modeled by the multiphase extension of Darcy's law,

$$\mathbf{u}_\ell = -\mathbf{K}\frac{k_\ell^{rel}}{\mu_\ell}\left(\nabla p_\ell - \rho_\ell g \nabla z\right), \tag{3.6}$$

where the subscript ℓ can denote either of the phases present in the system, and k_ℓ^{rel} is the *relative permeability* of phase ℓ. Since k_ℓ^{rel} represents the flux reduction due to a reduced effective pore volume, it is clear that k_ℓ^{rel} should be 1 if the pore volume is completely filled (or *saturated*) with the phase ℓ, and 0 if the phase is not present. When more than one phase is present, the value of k_ℓ^{rel} depend on the volume fraction (or *saturation*) of phase ℓ, but also on the distribution of phases within the rock. For instance, if the phase only occupies the smaller pores, the relative permeability is smaller than if the fluid occupies the larger pores. In practice, the dependence of relative permeability on saturation is determined by laboratory experiments.

When laboratory data on fracture relative permeability is not available, it is commonly assumed that the relative permeability is described by linear functions of the fluid saturation, as shown in Figure 3.1. This relationship is verified experimentally for two-phase flow in perfectly smooth-walled fractures, but for realistic, non-smooth fractures, the assumption of linear relative permeability curves is questionable [54].

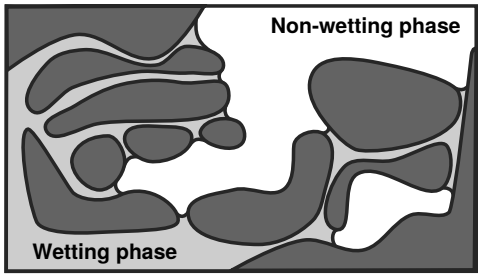

Figure 3.2: Typical distribution of wetting and non-wetting fluid. The wetting fluid adheres to the rock walls and enters the smaller pores first, possibly creating isolated pockets of trapped non-wetting fluid.

3.2.2 Capillary pressure

When two fluid phases are present within in the same porous rock, one of the phases will typically show a stronger attraction to the rock walls than the other. The phases with stronger and lesser rock wall attraction are called the *wetting fluid* and *non-wetting fluid*, respectively. Microscopically, the unequal attraction forces cause the wetting fluid to adhere to the rock walls, and move towards the portions of the rock with the smallest pore throats, as illustrated in Figure 3.2. Furthermore, there will be a pressure jump over the phase interface, which is known as the *capillary pressure*. The microscopic capillary pressure can be calculated from fluid properties and the diameter of the pore. The macroscopic definition of capillary pressure is slightly different, and can be thought of as the microscopic capillary pressure in the largest rock pore that is filled with wetting fluid [55]. Thus, it is a function of fluid saturation, and is usually determined experimentally.

Since the fracture apertures are typically much larger than the size of the pores, the capillary pressure in the fractures is small compared to the rock matrix. Thus, any wetting fluid entering the fracture space tends to migrate into the smaller pore space in the matrix, displacing the non-wetting fluid within. This *counter-current imbibition* process is an important oil recovery mechanism in water-wet fractured reservoirs, where injected water travels through the fractures and displaces the oil within the surrounding rock [20, 28].

3.2.3 Mass conservation

In a multiphase reservoir, one must keep track of the volume fluxes for each phase separately. Thus, there is a mass conservation equation similar to Equation (3.5) for each of the mobile phases in the reservoir,

$$\frac{\partial}{\partial t}\left(\phi S_\ell \rho_\ell\right) = -\nabla \cdot \left(\rho_\ell \mathbf{u}_\ell\right) + q_\ell, \tag{3.7}$$

where the subscript ℓ can denote either of the phases, and S_ℓ is the saturation of phase ℓ.

3.3 Dual continuum models

In some applications of flow in fractured geological formations, the fractured rock may behave as a regular porous rock with some special anisotropic characteristics. This is the case, for instance, if the rock matrix is impervious to flow, if there is only a single phase with negligible compressibility, or if there are two incompressible phases and capillary equilibrium is instantaneously obtained. In general, however, the rock matrix and the fracture network may behave as two separate, interacting media. Provided that the fracture network is amenable to upscaling (see Chapter 4), the interaction between the fracture network and the surrounding rock may be modeled by a *dual continuum* formulation.

3.3.1 Compressible flow

If the fluid within the porous rock is perfectly incompressible, changes in fluid pressure are instantaneous through the entire computational domain. In a realistic reservoir, changes in fluid pressure travels at a finite speed, dependent on both the fluid compressibility and the rock permeability. In a fractured rock, changes in fluid pressure travels much faster in the fractures than in the matrix due to higher permeability in the fractures.

This behavior becomes important when interpreting the results of hydraulic well tests. Consider for instance a pressure drawdown test, where a production well is shut down for some time, and then reopened for production at a constant pressure. While the well is shut, the fluid pressure in the reservoir stabilizes and the pressure within the fractures and the rock approaches equilibrium. Immediately after reopening the well, the fluid residing in the fractures flows towards the well at a high rate. This causes the pressure in the fractures to decline, which also reduces the flow rate. After some time, the fluid within the porous matrix starts to flow towards the fractures due to the pressure difference between the fractures and the matrix. This helps sustaining fluid flow, and slows down the pressure decline in the fractures.

To model the flow between fractures and matrix as described above, separate pressure variables are assigned to the fluids in the matrix and fractures. The mass flux between the two media is described by a *transfer function*, which in the simplest case is given as

$$\tau = \sigma\rho\frac{K_m}{\mu}\left(p_f - p_m\right), \tag{3.8}$$

where τ is the mass transfer rate per volume, K_m is the permeability of the matrix, μ is the fluid viscosity, ρ is the fluid mass density, p_f and p_m is the fluid pressure for the fractures and matrix, respectively, and σ is the *shape factor*, also called the *transfer coefficient* or *sigma factor* [71]. The shape factor is proportional to the square of the P32 fracture density (as defined in Section 2.3.1), but is also dependent on the variation in fracture orientation [57].

3.3.2 Two-phase flow

To correctly model the flow of separate fluid phases between the fractures and the porous matrix, a transfer function for each of the phases is needed. Assuming two phases, a wetting and non-wetting phase, the transfer functions are given as

$$\tau_w = \sigma \rho_w k_w^{rel} \frac{K_m}{\mu_w} \left(p_f - p_m \right), \tag{3.9}$$

$$\tau_n = \sigma \rho_n k_n^{rel} \frac{K_m}{\mu_n} \left(p_f - p_m + p_c \right), \tag{3.10}$$

where the subscripts w and n denote the wetting and non-wetting phases, respectively, k^{rel} is the relative permeability, p_f and p_m denote the wetting fluid pressure for the fractures and matrix, respectively, and p_c is the macroscopic capillary pressure [40]. Due to capillary pressure, the two transfer functions τ_w and τ_n commonly have opposite signs, representing a counter-current imbibition process.

If the capillary force is strong compared to the bulk velocity of fluid movement, the fluid transfer between fractures and matrix can be formulated as an equilibrium relation. In this case, the fractured rock behaves as a single-continuum material with a modified relative permeability relationship [44].

3.3.3 Mass conservation

In a dual continuum formulation, there are twice as many mass conservation equations compared with the single-continuum mass conservation equations (3.7), and the volume flux of fluids between the two continua appears as an extra source term. Using the superscripts m and f to denote the matrix and fractures, respectively, we get the following formulation:

$$\frac{\partial}{\partial t} \left(\phi^m S_\ell^m \rho_\ell^m \right) = -\nabla \cdot \left(\rho_\ell^m \mathbf{u}_\ell^m \right) + \tau_\ell + q_\ell^m, \tag{3.11}$$

$$\frac{\partial}{\partial t} \left(\phi^f S_\ell^f \rho_\ell^f \right) = -\nabla \cdot \left(\rho_\ell^f \mathbf{u}_\ell^f \right) - \tau_\ell + q_\ell^f, \tag{3.12}$$

where $\mathbf{u}$ refers to the volume flux of fluids within each continuum and τ is the mass transfer rate from the fractures to the matrix [40].

3.3.4 Heat flux

In geothermal reservoirs, the temperature of the fluid and surrounding rock is an important variable. If the fluid can not be assumed to be in thermal equilibrium with the rock, a heat transfer term similar to Equation (3.8) is defined,

$$\tau^{heat} = \sigma K_m^{heat} \left(T_f - T_m \right), \tag{3.13}$$

where τ^{heat} is the heat transfer rate per volume, σ is the shape factor, K_m^{heat} is the heat conductivity of the matrix, and T_f and T_m are the temperatures within the fracture and rock matrix, respectively [39].

3.4 Flow of electric currents

Electromagnetic techniques are often used to gain knowledge about the properties of a geological reservoir. Examples of such techniques are controlled-source electromagnetic surveys [15], borehole resistivity logging [38] and crosswell electromagnetic tomography [74]. To interpret the results of these methods, the flow of electrical currents within the reservoir must be modeled. A thorough description of mathematical models used for electromagnetic investigation techniques is beyond the scope of this section, but a short introduction to the governing equations is given below.

3.4.1 Maxwell's equations

Macroscopic electromagnetic processes are generally described by the macroscopic version of Maxwell's equations,

$$\nabla \cdot \mathbf{D} = \rho_e, \tag{3.14}$$

$$\nabla \cdot \mathbf{B} = 0, \tag{3.15}$$

$$\nabla \times \mathbf{E} = -\frac{\partial \mathbf{B}}{\partial t}, \tag{3.16}$$

$$\nabla \times \mathbf{H} = \mathbf{J} + \frac{\partial \mathbf{D}}{\partial t}, \tag{3.17}$$

where $\mathbf{E}$ is the *electric field intensity*, $\mathbf{B}$ is the *magnetic flux density*, $\mathbf{D}$ is the *electric flux density* or *displacement field*, $\mathbf{H}$ is the *magnetic field intensity* or *magnetizing field*, $\mathbf{J}$ is the *current density*, and ρ_e is the *charge density* for free electrical charges [41, 63]. For simple materials, the current density and the electrical field are related by *Ohm's law*,

$$\mathbf{J} = \boldsymbol{\sigma}\mathbf{E}, \tag{3.18}$$

where $\boldsymbol{\sigma}$ is the tensor-valued *electric conductivity*, which is a material constant.

The electric conductivity is an important parameter, since this is the material property that electromagnetic methods are the most sensitive to. In particular, since saline water has significantly higher conductivity than oil, electromagnetic methods are well-suited to distinguish between water-filled and oil-filled regions of a geological formation.

3.4.2 Stationary currents

In practice, electromagnetic methods are not sensitive to the pore-scale conductivity variations of the rock, but rather the *effective conductivity*. This is the average value of the electric conductivity within a certain volume depending on the resolution of the method. We return to the precise definition of effective conductivity in Section 4.1.2. Here, we merely state that the effective conductivity can be defined by considering stationary electromagnetic fields, i.e., fields that are time-invariant. In this case, the electric field $\mathbf{E}$ becomes irrotational (curl-free), and may therefore be represented by

a scalar potential function,

$$\mathbf{E} = \nabla\phi, \tag{3.19}$$

where ϕ is called the *electric potential*. Furthermore, by taking the divergence of Equation (3.17) and inserting Equation (3.18), we get the relation

$$0 = \nabla \cdot (\sigma \nabla\phi)\,. \tag{3.20}$$

Equation (3.20) is mathematically equivalent to the Laplace equation, and will be used in Section (4.1.2) to define effective conductivity.

Chapter 4

Upscaling of fracture permeability

Standard solution techniques for the equations presented in Chapter 3 require that the computational domain is subdivided into a finite number of cells, and a single value is used to represent the permeability within each of them. The size of the computational cell is determined by the required accuracy and the available computational power. In general, smaller cell sizes result in both higher accuracy and larger computational demand. With the computational capacity available to standard field-scale simulations, the lateral extent of a computational cell is typically chosen to be of the order of 100 m.

Ideally, fractures that are larger than the size of a typical computational cell should be represented explicitly in the numerical model, unless they are also closely spaced. This can be done by employing a *Discrete Fracture Matrix* (DFM) formulation [60], where the fractures are discretized by two-dimensional cells within an otherwise three-dimensional computational domain. But even if large fractures are separated from the rest of the model using a DFM formulation, the model may still contain a large amount of fractures that are smaller than the typical computational cell. This makes each cell highly heterogeneous in terms of permeability, and it is not trivial to find a single permeability value that is representative for the cell as a whole.

The process of obtaining a representative property value from a spatially heterogeneous material is called *upscaling* or *homogenization*. In this chapter, we first discuss how the representative permeability should be defined, by introducing the concept of *effective permeability*. For this concept to make sense, heterogeneous features within the material must be sufficiently small, and it is therefore only applicable if large-scale fractures have been removed using the DFM approach. In the second part of the chapter, we introduce two classes of analytical methods that can be used for estimating the effective permeability of fractured rocks, which is the *layer-based methods* and the *effective medium methods*. The accuracy and applicability of various effective medium methods is the topic of Paper A, B and C. In dual permeability models (see Section 3.3), the matrix and the fracture network must be upscaled independently, whereas the combined effective properties of matrix and fractures are required in a single continuum model.

4.1 Effective permeability

For applications to fluid permeability in porous rocks, it is appropriate to relate the concept of effective permeability to the average volume flux of an incompressible, single-phase fluid through the rocks [72]. Darcy's law for such a fluid is given by

$$\mathbf{u} = \mathbf{K}\frac{\rho g}{\mu}\nabla h, \tag{4.1}$$

where $h = p/\rho g + z$ is the *hydraulic head*. Combined with the mass conservation equation (3.5), this gives the *pressure equation* for an incompressible fluid in a porous medium with no mass sources,

$$\nabla \cdot \mathbf{K}\nabla h = 0. \tag{4.2}$$

In the above equation, we have factored out the fluid properties and the gravity constant, since they are all spatially invariant.

We now define the *effective permeability*[1] $\mathbf{K}_{eff}$ of a heterogeneous rock with permeability $\mathbf{K}$, as

$$\langle \mathbf{K}\nabla h \rangle = \mathbf{K}_{eff} \langle \nabla h \rangle , \tag{4.3}$$

where $\langle \cdot \rangle$ denotes the volume average over the domain, and h is any hydraulic head satisfying Equation (4.2). With this definition, the average fluid flux through the heterogeneous rock is equal to the average flux through a hypothetical homogeneous rock with permeability $\mathbf{K}_{eff}$ subject to the same boundary conditions. The effective permeability can therefore be used in a reservoir simulator as a representative value for the heterogeneous permeability within a computational cell.

4.1.1 Macroscopic homogeneity

For the effective permeability to be well-defined, Equation (4.3) should give consistent values for $\mathbf{K}_{eff}$ regardless of the boundary conditions. We refer to this property as *macroscopic homogeneity*. The assumption of macroscopic homogeneity is very strong, and does not strictly apply to heterogeneous finite-sized domains. A real material therefore has no effective permeability in the strict sense. It can still have an effective permeability in the approximate sense, meaning that Equation (4.3) holds exactly for a certain set of boundary conditions, and is approximately valid if the boundary conditions are changed. This is the definition of effective permeability most commonly used in field-scale applications of permeability upscaling.

4.1.2 Analogous physical properties

The concept of effective permeability can be extended to other physical properties as well. Mathematically, Equation (4.2) is equivalent to the Laplace equation, which

[1] As the term «effective permeability» has a slightly different meaning in the field of stochastic hydrology, the term «equivalent permeability» is often used in the literature to avoid confusion [72].

may be used to describe a number of physical phenomena. One example is the equation for stationary electrical currents in conductive media, Equation (3.20), introduced in Section 3.4.2. Similar to the effective permeability, we may define the *effective conductivity* $\boldsymbol{\sigma}_{eff}$ of a heterogeneous conductive medium as

$$\langle \boldsymbol{\sigma} \nabla \phi \rangle = \boldsymbol{\sigma}_{eff} \langle \nabla \phi \rangle \,, \tag{4.4}$$

where ϕ is any electric potential satisfying Equation (3.20). With this definition, the average current density though the heterogeneous medium is equal to the average current density through a hypothetical homogeneous medium with conductivity $\boldsymbol{\sigma}_{eff}$, subject to the same boundary conditions.

In the remainder of this chapter, upscaling methods for fractured media are discussed using terminology from fluid flow in porous media. However, it is important to keep in mind that the same methods are applicable to electrical conductivity as well, due to the mathematical analogy described above. Other effective properties that can be defined in an analogous way include the effective thermal conductivity and the effective diffusion coefficient [68].

4.1.3 Numerical upscaling

Given an explicit description of the heterogeneous permeability field within a grid block, it is possible to find its effective permeability numerically. One approach is to first solve Equation (4.2) for the heterogeneous material using periodic boundary conditions, with an applied head gradient along one of the main directions of the grid block. Finally, equation (4.3) is applied to compute the value of $\mathbf{K}_{eff}$ along the direction of the gradient. This procedure is repeated for the other main directions of the grid block, until all components of $\mathbf{K}_{eff}$ has been computed.

If the principal directions of $\mathbf{K}_{eff}$ are known to be aligned with the grid block, $\mathbf{K}_{eff}$ can also be found by specifying a fixed hydraulic head on two opposing sides, and apply no-flow conditions on the remaining block faces. Even more methods for estimating $\mathbf{K}_{eff}$ numerically are summarized by [72].

Numerical upscaling gives an accurate estimate of the effective permeability provided that a fine, high-quality mesh is used. The disadvantage of the approach is the computational effort required, which can be very demanding for applications to fractured media.

4.1.4 Stochastically defined materials

In a fractured geological reservoir, the exact location, size and orientation of the fractures are often unknown. Instead, the fracture geometry is specified by statistical parameters and probability distributions, which makes the permeability field a stochastic quantity. Thus, to find the effective permeability by numerical means, one must generate a realization of the fracture geometry, and compute the corresponding effective permeability of the realization. If the medium is infinitely extending and *ergodic* (meaning that a volume average can replace an ensemble average), any realization

Figure 4.1: Layered medium.

of the material gives the same effective permeability [68]. Since a real, finite-sized medium does not meet these criteria exactly, one should find the effective permeability of several different realizations and compute the average of the results, in order to find a representative permeability value for the material.

4.2 Layer-based upscaling models

Numerical upscaling of a fractured material is computationally very expensive, since an accurate solution of the pressure equation (4.2) for a three-dimensional fractured medium requires a very fine mesh and the solution of a large linear system. Thus, analytical estimates of the effective permeability are attractive, even if they are less accurate than numerical methods. In this section, we introduce the simple harmonic and arithmetic averaging techniques, and show how they may be useful for applications to fractured media.

4.2.1 The arithmetic and harmonic average

To derive the equation for the arithmetic average, suppose that we have a layered material as depicted in Figure 4.1, with isotropic permeability within each layer. Let K_i and ϕ_i denote the permeability and volume fraction, respectively, of layer i. Also, suppose that a fixed hydraulic head difference is prescribed between the left and right side, and assume periodic boundary conditions for the remaining sides. By solving the pressure equation (4.2) for this configuration, and applying Equation (4.3), we find that the effective permeability in the horizontal direction is

$$K_{eff,hor} = \phi_1 K_1 + \phi_2 K_2. \tag{4.5}$$

It can be shown that the arithmetic average represent the upper bound for the effective permeability, for any mixture of the two materials K_1 and K_2 [68].

Similarly, to derive the harmonic average, suppose that we change the boundary conditions such that there is a fixed hydraulic head difference between the top and bottom face, and periodic boundary conditions on the remaining sides. By solving the pressure equation (4.2) and applying Equation (4.3), we find that the effective

permeability in the vertical direction is given by

$$\frac{1}{K_{eff,ver}} = \frac{\phi_1}{K_1} + \frac{\phi_2}{K_2}. \tag{4.6}$$

Just as the arithmetic average is an upper bound for the effective permeability, the harmonic average represent a lower bound for the effective permeability of any mixture of the materials K_1 and K_2 [68].

Merging the two results above, we arrive at the expression for the anisotropic effective permeability of layered media,

$$\mathbf{K}_{eff} = K_{eff,hor}\left(\mathbf{I} - \mathbf{nn}^\top\right) + K_{eff,ver}\,\mathbf{nn}^\top, \tag{4.7}$$

where $\mathbf{I}$ is the identity matrix, $\mathbf{n}$ is the unit normal vector for the layers and $\mathbf{nn}^\top$ denotes the outer product. The expression is valid even for repeated, aligned layers with uneven layer spacing [68].

Equation (4.7) can be used to estimate the effective permeability of a fractured medium where all the fractures are infinitely extending and aligned in the same direction. Since fractures are very thin, it may be appropriate to set the volume fraction of the matrix material to 1, in which case the formulas can be rewritten as

$$K_{eff,hor} = aAK_f + K_m, \tag{4.8}$$

$$\frac{1}{K_{eff,ver}} = \frac{aA}{K_f} + \frac{1}{K_m}, \tag{4.9}$$

where K_f is the fracture permeability, K_m is the matrix permeability, a is the fracture aperture, and A is the fracture surface area per rock volume, i.e., the P32 fracture density (see Section 2.3.1). In the case of open fractures, we have $K_{eff,ver} \approx K_m$, since $aA \ll K_f/K_m$. Similarly, for cemented fractures, we have $K_{eff,hor} \approx K_m$ since $aAK_f \ll K_m$.

4.2.2 Non-aligned layers

Equation (4.7) can be extended by superposition to materials with layers in different directions, provided that the layers are thin [52, 66, 68]. For open fractures, this results in the formula

$$\mathbf{K}_{eff} = \mathbf{K}_m + \sum_{i=1}^{N} a_i A_i K_{f,i}\left(\mathbf{I} - \mathbf{n}_i\mathbf{n}_i^\top\right), \tag{4.10}$$

where N is the number of fracture sets, and a_i, A_i, $K_{f,i}$, $\mathbf{n}_i$ denote the aperture, surface area per volume, permeability and unit normal, respectively, for the fracture set i. The permeability contribution in the fracture normal direction is neglected since it is assumed that the fractures are thin. The equivalent of Equation (4.10) for cemented fractures is

$$\mathbf{K}_{eff}^{-1} = \mathbf{K}_m^{-1} + \sum_{i=1}^{N} \frac{a_i A_i}{K_{f,i}} \mathbf{n}_i\mathbf{n}_i^\top. \tag{4.11}$$

If there is a continuous distribution of fracture orientations, the summation in Equations (4.10) and (4.11) are replaced by an integral.

4.2.3 Partially connected fractures

A simple way of extending Equations (4.10) and (4.11) to fractures that are not infinite in size, is to introduce the connectivity parameter f, which scales the permeability of the fracture network according to the connectivity of the network. Applied to open fractures, we have

$$\mathbf{K}_{eff} = \mathbf{K}_m + f \sum_{i=1}^{N} a_i A_i K_{f,i} \left(\mathbf{I} - \mathbf{n}_i \mathbf{n}_i^\top \right), \tag{4.12}$$

and for cemented fractures we have

$$\mathbf{K}_{eff}^{-1} = \mathbf{K}_m^{-1} + f \sum_{i=1}^{N} \frac{a_i A_i}{K_{f,i}} \mathbf{n}_i \mathbf{n}_i^\top. \tag{4.13}$$

Various ways of estimating f analytically for open fractures are given by [31, 33, 48, 50]. On the other hand, less is known about the relationship between f and fracture parameters in the cemented case.

4.3 Inclusion-based upscaling models

Layer-based upscaling methods starts with the assumption that the fractures are infinitely extending and modifies the resulting expressions to account for partially connected fractures. Inclusion-based upscaling methods can be viewed as the opposite approach; assume that the fractures are infinitely well separated and modify the resulting expressions to account for interactions between the fractures. For this strategy to be successful, a way of calculating the impact of a single fracture on permeability is needed. It turns out that the impact of a single fracture can be calculated analytically if the fracture is shaped as a thin ellipsoid. For this reason, most inclusion-based upscaling methods assume that the fractures have ellipsoidal shapes.

4.3.1 Single inclusion problem

The single inclusion problem can be formulated as finding the average pressure gradient $\langle \nabla p \rangle$ through an ellipsoidal inclusion with intrinsic permeability $\mathbf{K}$, which is embedded in a matrix of homogeneous permeability $\mathbf{K}_m$ and subject to an externally applied pressure gradient ∇p_{far} (see Figure 4.2). It turns out that the pressure gradient within the inclusion is actually constant under these conditions, and linearly dependent on the externally applied pressure. By solving the pressure equation (4.2) in spherical coordinates [19, 41, 68], the solution is found to be

$$\nabla p = \mathbf{R} \nabla p_{far}, \tag{4.14}$$

where $\mathbf{R}$ is the *field concentration tensor*, given by

$$\mathbf{R} = \left(\mathbf{I} + \mathbf{K}_m^{-\frac{1}{2}} \mathbf{A} \mathbf{K}_m^{-\frac{1}{2}} \left(\mathbf{K} - \mathbf{K}_m \right) \right)^{-1}. \tag{4.15}$$

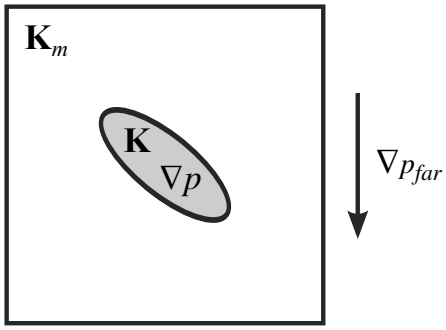

Figure 4.2: Single inclusion problem. The background material is homogeneous with permeability $\mathbf{K}_m$, the inclusion has permeability $\mathbf{K}$. The pressure gradient ∇p within the inclusion is constant and linearly dependent on the externally applied pressure gradient ∇p_{far}, as given by Equation (4.14).

In the above expression, $\mathbf{A}$ is the *depolarization tensor*, which is dependent on the shape and orientation of the ellipsoidal inclusion, as well as the anisotropy of the background permeability $\mathbf{K}_m$.

If $\mathbf{K}_m$ is isotropic, the depolarization tensor $\mathbf{A}$ is oriented along the axes of the ellipsoidal inclusion, with eigenvalues (*depolarization factors*) given by

$$A_i = \frac{r_1 r_2 r_3}{2} \int_0^\infty \frac{dt}{\left(t + r_i^2\right) \sqrt{\left(t + r_1^2\right)\left(t + r_2^2\right)\left(t + r_3^2\right)}}, \tag{4.16}$$

where r_1, r_2 and r_3 are the half-axis lengths of the ellipsoid. Equation (4.16) is a *symmetric elliptic integral* of the second kind, which may be calculated using duplication [11] or half- and double-argument transformations [26].

If $\mathbf{K}_m$ is anisotropic, the values of r_1, r_2 and r_3 in Equation (4.16), as well as the eigenvectors of $\mathbf{A}$, depend on the degree of anisotropy as shown in [5] and in Paper B.

4.3.2 Dilute limit approximation

For a material containing well-separated ellipsoidal inclusions, the average volume flux through the medium is found by splitting the domain into many single inclusion problems and adding the contributions of each inclusion as given by Equation (4.14). With the assumption that the inclusions do not interact, the definition of effective permeability (4.3) can thus be applied directly. This gives the dilute limit approximation,

$$\mathbf{K}_{eff} = \mathbf{K}_m + \sum_{i=1}^{N} \phi_i \left(\mathbf{K}_i - \mathbf{K}_m\right) \mathbf{R}_i, \tag{4.17}$$

where the subscript i denote the inclusion family (determined by the inclusion shape, size, orientation and permeability), and ϕ_i, $\mathbf{K}_i$, $\mathbf{R}_i$ are the volume fraction, permeability and field concentration tensor, respectively, of inclusion family i. As before, $\mathbf{K}_{eff}$

is the effective permeability, and $\mathbf{K}_m$ is the permeability of the matrix. Details on the derivation of Equation (4.17) may be found, for instance, in [36, 56], as well as in Paper B.

4.3.3 Effective medium methods

Effective medium methods are a group of upscaling methods based on the dilute limit approximation that account for interactions between inclusions to some degree. Some of the more popular variants are the differential method, the symmetric and asymmetric self-consistent methods, the Maxwell approximation and the cluster expansion methods, although the latter group is not always classified as an effective medium method. Within the included Paper B and C, reviews of different effective medium methods are given, and adapted for applications to fractured media. More comprehensive introductions to general effective medium theory are given in [46, 68].

Chapter 5

Ensemble-based parameter inversion

Although most fracture parameters can be measured, the measurements have a high degree of uncertainty. Consequently, there may be a mismatch between the predicted and actual well flow rates and fluid composition. A similar mismatch may also be observed for other data types, such as the seismic response. History matching methods make use of this discrepancy to adjust the reservoir model and improve its predictive value.

The last of the included papers, Paper D, is concerned with the interplay between upscaling and history matching of fractured reservoirs. The paper focuses on ensemble-based history matching methods, which have gained popularity in recent years. As a background for the paper and the methods therein, this chapter provides a short introduction to inverse modeling and different variants of ensemble-based parameter inversion.

5.1 The inverse problem

History matching is the process of adjusting the parameters of the reservoir model such that the measured flow rates, fluid temperature and fluid composition agree with the predictions of the model. More generally, reservoir history matching can be viewed as an *inverse problem*. To define this term, assume that we have a mathematical model, possibly simplified, describing some physical process with a measurable outcome. Furthermore, assume that the model is dependent on some physical parameters that are unknown or uncertain. The inverse problem can be formulated as estimating the parameters of the mathematical model using the measured outcome of the physical process. In other words, we are concerned with finding the parameters $\mathbf{y}$, given implicitly as

$$\mathbf{F}(\mathbf{y}) = \mathbf{d} + \boldsymbol{\epsilon}, \tag{5.1}$$

where $\mathbf{F}$ represents the mathematical model of the physical process, $\mathbf{d}$ is the measured data and $\boldsymbol{\epsilon}$ represents the measurement noise and model uncertainty.

5.1.1 Direct inversion methods

Direct inversion methods make use of optimization algorithms to minimize the mismatch between the predicted and actual measurements,

$$\tilde{\mathbf{y}} = \operatorname{argmin} \|\mathbf{F}(\mathbf{y}) - \mathbf{d}\|^2 + T(\mathbf{y}), \tag{5.2}$$

where $\tilde{\mathbf{y}}$ are the estimated parameters and T is a regularization function, which is applied to avoid letting the measurement noise have too much influence on the solution. In the case of simple *Tikhonov regularization* [2], T is given as

$$T(\mathbf{y}) = \gamma \|\mathbf{y}\|^2, \tag{5.3}$$

where γ is a regularization parameter that is dependent on the noise level.

Direct inversion methods differ in which optimization algorithm is used, the way they regularization term is formulated, and how the degree of regularization is determined. An introduction to various methods for direct inversion is given by [2].

5.1.2 Bayesian inversion methods

Unlike direct methods, *Bayesian inversion methods* may be used to find both a parameter estimate and an uncertainty estimate, since they are based on a probabilistic formulation. Moreover, they are also able to take prior parameter information into account. An introduction to general Bayesian inversion is given by [53].

The goal of Bayesian methods is to estimate the *posterior parameter distribution* according to Bayes' theorem,

$$p(\mathbf{y}|\mathbf{d}) = \frac{p(\mathbf{d}|\mathbf{y})\, p(\mathbf{y})}{p(\mathbf{d})}, \tag{5.4}$$

where $p(\mathbf{y}|\mathbf{d})$ is the probability density for the posterior distribution, $p(\mathbf{d}|\mathbf{y})$ is the *likelihood*, $p(\mathbf{y})$ is the probability density for the *prior parameter distribution* and $p(\mathbf{d})$ can be interpreted as a normalization factor. The likelihood is the probability density for a measurement outcome $\mathbf{d}$, given a certain set of parameters $\mathbf{y}$. The prior distribution represents our initial knowledge on likely parameter values, before any measurement is made.

A common way of representing a multidimensional parameter distribution, is by drawing a random sample from the distribution. If the number of parameters is small, Equation (5.4) can be sampled using the rejection algorithm or a similar sampling algorithm [53]. If the number of parameters is large, however, direct sampling of Equation (5.4) becomes computationally very expensive. This is because multidimensional integrals are difficult to evaluate when the number of dimensions is large, a fact known as the *curse of dimensionality*.

5.2 The Ensemble Kalman Filter and related methods

The *Ensemble Kalman Filter* (EnKF) is a Bayesian inversion method that approximates the posterior distribution by assuming that the distribution is approximately

Gaussian. A detailed derivation of the method is given, for instance, in [1, 53]. The method has gained popularity because of its modest computational requirements, ease of implementation, and relative robustness in reservoir applications.

5.2.1 Sequential assimilation

Applications of the EnKF begin by defining a *prior ensemble*, which is a random sample of parameter values from the prior distribution. The static parameters and the dynamic state variables are jointly organized in a matrix $\boldsymbol{M}$, where each column of $\boldsymbol{M}$ represents an ensemble member. A reservoir simulator is then applied to each ensemble member, to produce a set of *data variables* such as fluid pressure and composition within wells. This is the *forecast stage*. The data variables are assembled into a matrix $\boldsymbol{D}$, where each column represents data from a single simulation.

After the forecast step, the data variables are compared with physical measurements, and the mismatch is used to adjust the model variables. This is the *assimilation stage*. The following formula is used, which is an ensemble-based approximation of Equation (5.4) for Gaussian distributions [53],

$$\begin{aligned} \boldsymbol{M}_{\text{post}} &= \boldsymbol{M} + \boldsymbol{M}_{\text{diff}}, \\ \boldsymbol{M}_{\text{diff}} &= \Delta \boldsymbol{M} \Delta \boldsymbol{D}^{\top} \left[\boldsymbol{C}_D + \Delta \boldsymbol{D} \Delta \boldsymbol{D}^{\top} \right]^{-1} \boldsymbol{D}_{\text{diff}}, \\ \boldsymbol{D}_{\text{diff}} &= \boldsymbol{D}_{\text{obs}} - \boldsymbol{D} + \epsilon, \end{aligned} \tag{5.5}$$

where $\boldsymbol{M}_{\text{post}}$ is an ensemble representing the posterior distribution, $\boldsymbol{C}_D$ is the covariance matrix for the data noise, $\boldsymbol{D}_{\text{obs}}$ is a vector of actual measurement data, and ϵ is a matrix of realized data noise (i.e., artificial Gaussian noise with covariance $\boldsymbol{C}_D$). The operator Δ denotes a square root of the ensemble covariance, defined by

$$\Delta \boldsymbol{M} = \frac{\boldsymbol{M} - \overline{\boldsymbol{M}}}{\sqrt{N-1}}, \tag{5.6}$$

where $\overline{\boldsymbol{M}}$ is the ensemble mean of $\boldsymbol{M}$, and N is the number of ensemble members.

An illustration of the EnKF procedure is given in Figure 5.1. In standard applications of the EnKF, data are assimilated sequentially in time, applying Equation (5.5) at each time step where data is available. Note that dynamic state variables such as pressure and saturation are included in the ensemble matrix $\boldsymbol{M}$, and are adjusted at each data assimilation step. The adjusted state variables then become initial conditions for the next forecast stage.

5.2.2 Simultaneous assimilation

A problem with including state variables in the ensemble matrix $\boldsymbol{M}$, is that the assimilation step may introduce inconsistencies to the solution, such as the loss of mass conservation. It may also introduce an artificial spatial roughness in the state variables, which makes it difficult to restart the simulation after a data assimilation step. The problem can be avoided by assimilating all the measured data, from all time steps,

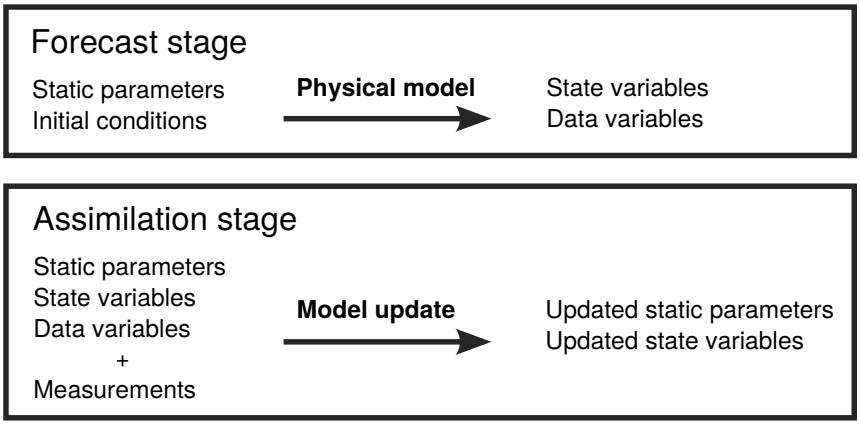

Figure 5.1: The forecast and assimilation stages of the Ensemble Kalman Filter. The state variables and data variables computed in the forecast step are used as input in the assimilation step, where Equation (5.5) is used to update the model. The updated state variables are used as initial conditions for the next forecast step.

in a single step at the end of the numerical simulation. This is the *ensemble smoother* method [65], which is also called *simultaneous assimilation*. With this approach, one does not have to estimate the state variables, and the problem of restarting the simulation from unphysical parameters is eliminated. The major disadvantage of the method is that the ensemble smoother is much more sensitive to model nonlinearities than the sequential EnKF [25]. Therefore, it is often coupled with iterative schemes as described in the following sections.

5.2.3 Multiple Data Assimilation

The *Multiple Data Assimilation* (MDA) scheme [18] is an iterative version of Equation (5.5) that performs better for nonlinear models. The update formula is given by

$$\begin{aligned} M_i &= M_{i-1} + M_{\mathrm{diff},i}, \\ M_{\mathrm{diff},i} &= \Delta M_i \Delta D_i^{\top} \left[n C_D + \Delta D_i \Delta D_i^{\top} \right]^{-1} D_{\mathrm{diff},i}, \\ D_{\mathrm{diff},i} &= D_{\mathrm{obs}} - D_i + \epsilon_i, \end{aligned} \tag{5.7}$$

where i is the iteration index, and n is the number of iterations, which must be determined beforehand. The scheme can be applied to both sequential and simultaneous data assimilation. If the prior distribution is Gaussian and the simulation model is linear, Equation (5.7) samples the posterior distribution correctly regardless of the number of iterations.

5.2.4 Ensemble Randomized Maximum Likelihood

Another scheme for iterative data assimilation is the *Ensemble Randomized Maximum Likelihood* (EnRML) method [12]. Unlike the MDA algorithm, the number of

iterations is not predefined, and the iterations can be terminated at any time due to a data mismatch criterion. Since the EnRML is formulated as an optimization scheme, there are several variants of the method depending on the optimization algorithm used [12, 13]. When used in conjunction with the Levenberg-Marquard scheme, the update formula is given by

$$\begin{aligned} M_{i+1} &= M_i + M_{\mathrm{diff},i} + M_{\mathrm{corr},i}, \\ M_{\mathrm{diff},i} &= \Delta M_i \Delta D_i^{\top} \left[\left(1+\lambda_i\right) C_D + \Delta D_i \Delta D_i^{\top} \right]^{-1} \left(D_{\mathrm{obs}} - D_i + \epsilon_i \right), \\ M_{\mathrm{corr},i} &= \Delta M_i \left[\left(1+\lambda_i\right) I + \Delta D_i^{\top} C_D^{-1} \Delta D_i \right]^{-1} \Delta M_i^{\top} C_{M_0}^{-1} \left(M_0 - M_i \right), \end{aligned} \tag{5.8}$$

where λ_i is the Levenberg-Marquard regularization parameter, and C_{M_0} is the covariance matrix for the prior ensemble. The term $M_{\mathrm{corr},i}$ represents a correction factor, ensuring that the posterior distribution estimate does not deviate too much from the prior distribution.

In practical computations, several of the terms in Equation (5.8) should be computed using a scaled truncated singular value decomposition (TSVD) for better numerical stability, as described by [13]. In particular, the inverse of the prior covariance matrix C_{M_0} is difficult to estimate without using a TSVD, since the standard ensemble estimate of C_{M_0} does not have full rank.

Chapter 6

Introduction to the papers

This chapter provides an introduction to the included papers, all of which are either published or submitted for publication in scientific journals. The author of this thesis is also the first author of the papers. The co-authors have contributed by providing research directions through scientific discussions, and by giving valuable suggestions on how to improve the manuscripts.

6.1 Paper A and B

Paper A

Title:	*Electrical conductivity of fractured media: A computational study of the self-consistent method*
Authors:	P. N. Sævik, I. Berre, M. Jakobsen and M. Lien
Journal:	In SEG Technical Program Expanded Abstracts (2012)

Paper B

Title:	*A 3D Computational Study of Effective Medium Methods Applied to Fractured Media*
Authors:	P. N. Sævik, I. Berre, M. Jakobsen and M. Lien
Journal:	Transport in Porous Media 100, 1 (2013)

Paper A and B assess the potential of effective medium theory for estimating macroscopic properties of fractured rocks. The use of effective medium methods for this purpose was previously suggested by a number of authors [5, 7, 23, 56], but the quality of the estimates has been questioned [31, 68]. This is partly due to the lack of analytical error estimates, and partly because the microgeometry of a densely fractured rock is very different from the geometries where effective medium theory is known to be reliable.

In Paper A and B, predictions from effective medium theory is compared with results from numerical upscaling. Thus, the papers represent a valuable contribution to determining if effective medium theory is applicable to fractured media. Paper A contains preliminary results, where estimates from the asymmetric self-consistent method

is compared with numerical upscaling for two orthogonal fracture sets. In Paper B, the full set of numerical results is presented, and used to assess the accuracy of three different classes of effective medium methods. For comparison, Paper B also includes the semi-analytical method of Mourzenko et al [50], which is based on principles that are fundamentally different from effective medium theory. Paper A is presented in the context of electrical conductivity, whereas Paper B is presented in the context of fluid permability.

The numerical computations are performed on randomly distributed, equisized disc-shaped fractures with predefined orientations. By a simple scaling of the results, this geometrical configuration is also representative for fractures with polygonal shape and a power-law size distribution [49]. Two types of numerical computations are performed: Finite-element computations to determine the effective permeability or conductivity, and topological computations to determine the percolation threshold of different configurations.

The papers also address a problem with traditional effective medium formulas when applied to fractured media, namely, that they become numerically unstable for flat inclusions. This problem is solved by introducing a novel reformulation of the standard equations, which is numerically stable even in the limit of zero thickness. The new formulas show fast and reliable convergence behavior for isotropic and anisotropic media, below and above the percolation threshold, for all levels of matrix/fracture permeability contrast. Furthermore, they require a smaller number of input variables compared with the traditional formulation when applied to thin inclusions. Traditional formulations require both the thickness and the permeability of the inclusion to be specified, but the reformulated equations reveal that the effective permeability is only sensitive to the product (for open fractures) or quotient (for cemented fractures) of these quantities.

For open fractures, our results show that self-consistent methods, especially the asymmetric variant, may be used to give reasonable estimates of the effective conductivity even beyond the percolation threshold. The symmetric variant gives the best estimate just above the threshold, but has the wrong asymptotic behaviour for large fracture densities. For non-percolating geometries, or when the fracture/matrix conductivity contrast is small, all effective medium methods are performing well, and the differential method is marginally the best estimator. The semi-analytical method of Mourzenko et al. [50] usually gives the most accurate results whenever it is applicable, i.e., high-density networks of conductive fractures with equal transmissitivities. In the case of cemented fractures, our numerical simulations only cover fracture densities below the void percolation threshold. Within this range, the differential method is seen to give the best estimate. For high fracture densities, the self-consistent methods predict percolation thresholds that are well below the theoretical value, and the differential method has no percolation threshold at all.

A somewhat surprising result was the close agreement between numerically computed percolation thresholds and the thresholds predicted by the asymmetric self-consistent method. The self-consistent percolation estimates also scaled well with changes in the fracture intersection angle. Previously, it was unknown whether or

not these estimates were useful, since there are no theoretical results linking the self-consistent percolation estimates to the true percolation threshold of finite-sized fractures. Our results show that the asymmetric self-consistent method can give a very good indication of the percolation threshold for a large range of fracture configurations.

6.2 Paper C

Title:	*Anisotropic effective conductivity in fractured rocks by explicit effective medium methods*
Authors:	P. N. Sævik, M. Jakobsen, M. Lien and I. Berre
Journal:	Geophysical Prospecting 62, 6 (2014)

The effective medium methods considered in Paper A and B are *implicit*, meaning that the analytical estimates are defined by implicit equations that must be solved using iterative methods. In contrast, Paper C is concerned with *explicit* methods, where the estimates can be calculated directly from an explicit formula. As in Paper A, the methods are discussed in the context of electrical conductivity.

Explicit methods are easy to use and implement, they are computationally efficient, and it is possible to obtain analytical derivatives, which may be important in optimization applications. On the other hand, the methods are not applicable to media that are both strongly heterogeneous and strongly anisotropic. Two existing explicit methods are considered in the paper, namely, the Maxwell approximation [45, 68] and the T-matrix method [36, 37]. In addition, three novel explicit schemes for anisotropic media are constructed, based on the weakly self-consistent assumption previously suggested by Berryman and Hoversten [7].

In the original paper by Berryman and Hoversten, the weakly self-consistent assumption was applied only to the asymmetric self-consistent method, and the resulting expression was solved iteratively, for conductive fractures only. In Paper C, we show that the assumption is applicable to both the symmetric and asymmetric self-consistent method, as well as the differential method. We also show how the resulting expressions can be evaluated explicitly, for both conductive and resistive fractures.

Similar to the procedure used in Paper A and B, the methods considered in Paper C are reformulated and adapted for applications to thin inclusions. To assess the accuracy of the methods, conductivity estimates are compared with theoretical upper and lower bounds, theoretical percolation thresholds and asymptotic bounds, as well as numerical simulations.

The analysis in Paper C shows that the asymmetric variant of the weakly symmetric self-consistent method has the correct asymptotic behavior and satisfies all bounds, whereas the symmetric variant does not. This holds even in the isotropic case, where the weakly self-consistent methods coincide with the original implicit methods. The result is surprising, since the symmetric method is regarded to have a stronger theoretical foundation than the asymmetric one [6, 7, 47, 68]. Specifically, it has been proven

that the symmetric method is a *physically realizable* scheme, and should therefore not show unphysical behavior [3, 46]. A possible explanation is that the proof of realizability is not applicable to the special geometry that a fracture-matrix system represents, but further research is required in order to confirm this.

The comparisons between analytical and numerical results show that all the methods give accurate estimates for small fracture densities. For high densities and large matrix/fracture conductivity contrasts, all but the weakly self-consistent methods break down. Furthermore, the analysis in the paper shows that the weakly self-consistent methods predict percolation thresholds that are independent of fracture orientation, which is a gross oversimplification in the anisotropic case. We show that one remedy is to scale the result by a given percolation threshold, which may be estimated using other techniques. The resulting estimate is seen to agree closely with the original implicit self-consistent estimate. The scaling technique can not be used for non-percolating geometries, such as aligned fractures or, in the resistive case, geometries with less than three linearly independent fracture orientations. In these situations, the weakly self-consistent methods fails completely at high densities.

6.3 Paper D

Title:	*An Integrated Approach to Upscaling and History Matching of Fractured Media*
Authors:	P. N. Sævik, M. Lien and I. Berre
Journal:	Submitted to Water Resources Research (2015)

In Paper D, we investigate a particular problem that may occur when fracture upscaling methods are used together with history matching. Upscaling is commonly performed as a separate step prior to history matching, while the subsequent inversion algorithm uses upscaled parameters as primary variables. Paper D shows that this approach may lead to parameter combinations that are inconsistent with the underlying fracture description. Instead, we suggest in this paper to perform history matching on the fracture parameters directly, and include fracture upscaling as an integral part of the history matching workflow. This approach has an added computational cost, but if analytical upscaling methods are used, the added computational work is negligible.

The issues highlighted in Paper D are relevant to a number of physical applications, such as geothermal reservoirs, CO_2 storage and groundwater contamination problems, but the paper focuses primarily on applications to two-phase flow in petroleum reservoirs. Furthermore, we focus on the Ensemble Kalman Filter class of history matching methods, and use the analytical permeability upscaling method by Mourzenko et al [50]. Issues similar to the ones discussed in the paper are expected to arise with other method choices as well, such as Occam's razor and other direct methods for history matching [2], and the effective medium methods from Paper A, B and C for permeability upscaling.

We demonstrate the difference between the traditional and our proposed approach using simple numerical examples, as well as a synthetic field case based on the PUNQ-S3 model [22]. The simpler numerical examples are used to demonstrate that parameter inconsistencies does not appear for linear fracture upscaling relations, since the Ensemble Kalman Filter class of methods are invariant under linear variable changes. In particular, it is shown that upscaling of fully connected and randomly oriented fracture networks is linear if logarithmic variables are used.

The results from the field case show that the use of upscaled parameters as primary inversion variables does not only generate inconsistent parameter values, but may also make it difficult to match data. In our example, the inversion algorithm was able to match the data from all the wells only if fracture parameters were used as primary variables. When upscaled parameters were used as inversion variables, the posterior ensemble spread was significantly larger than the measurement uncertainty, and some well data could not be matched at all.

Bibliography

[1] Aanonsen, S. I., Nævdal, G., Oliver, D. S., Reynolds, A. C., and Vallès, B. The Ensemble Kalman Filter in Reservoir Engineering–a Review. *SPE Journal 14*, 03 (2009), 393–412. doi: 10.2118/117274-PA.

[2] Aster, R. C., Borchers, B., and Thurber, C. H. *Parameter Estimation and Inverse Problems*, 1 ed. Elsevier Inc., 2005.

[3] Avellaneda, M. Iterated homogenization, differential effective medium theory and applications. *Communications on Pure and Applied Mathematics 40*, 5 (1987), 527–554. doi: 10.1002/cpa.3160400502.

[4] Balberg, I., Alexander, S., and Wagner, N. Excluded volume and its relation to the onset of percolation. *Physical Review B 30*, 7 (1984), 3933–3943. doi: 10.1103/PhysRevB.30.3933.

[5] Barthélémy, J.-F. Effective Permeability of Media with a Dense Network of Long and Micro Fractures. *Transport in Porous Media 76*, 1 (2008), 153–178. doi: 10.1007/s11242-008-9241-9.

[6] Berryman, J. G., and Berge, P. A. Critique of two explicit schemes for estimating elastic properties of multiphase composites. *Mechanics of Materials 22*, 2 (1996), 149–164. doi: 10.1016/0167-6636(95)00035-6.

[7] Berryman, J. G., and Hoversten, G. M. Modelling electrical conductivity for earth media with macroscopic fluid-filled fractures. *Geophysical Prospecting 61*, 2 (2013), 471–493. doi: 10.1111/j.1365-2478.2012.01135.x.

[8] Bonnet, E., Bour, O., Odling, N. E., Davy, P., Main, I., Cowie, P., and Berkowitz, B. Scaling of fracture systems in geological media. *Reviews of Geophysics 39*, 3 (2001), 347–383. doi: 10.1029/1999RG000074.

[9] Bruggeman, D. A. G. Berechnung verschiedener physikalischer Konstanten von heterogenen Substanzen. I. Dielektrizitätskonstanten und Leitfähigkeiten der Mischkörper aus isotropen Substanzen. *Annalen der Physik 416*, 7 (1935), 636–664. doi: 10.1002/andp.19354160705.

[10] Cacas, M. C., Daniel, J. M., and Letouzey, J. Nested geological modelling of naturally fractured reservoirs. *Petroleum Geoscience 7*, S (2001), S43–S52. doi: 10.1144/petgeo.7.S.S43.

[11] Carlson, B. C. Numerical computation of real or complex elliptic integrals. *Numerical Algorithms 10*, 1 (1995), 13–26. doi: 10.1007/BF02198293.

[12] Chen, Y., and Oliver, D. S. Ensemble Randomized Maximum Likelihood Method as an Iterative Ensemble Smoother. *Mathematical Geosciences 44*, 1 (2011), 1–26. doi: 10.1007/s11004-011-9376-z.

[13] Chen, Y., and Oliver, D. S. Levenberg-Marquardt forms of the iterative ensemble smoother for efficient history matching and uncertainty quantification. *Computational Geosciences 17*, 4 (2013), 689–703. doi: 10.1007/s10596-013-9351-5.

[14] Chiles, J. P., and de Marsily, G. Stochastic models of fracture systems and their use in flow and transport modeling. In *Flow and Contaminant Transport in Fractured Rocks*, J. Bear, C.-F. Tsang, and G. de Marsily, Eds. Academic Press, Inc., San Diego, California, 1993, ch. 4, pp. 169–236. doi: 10.1016/B978-0-12-083980-3.50008-5.

[15] Constable, S. Ten years of marine CSEM for hydrocarbon exploration. *Geophysics 75*, 5 (2010), 75A67. doi: 10.1190/1.3483451.

[16] de Marsily, G. *Quantitative hydrogeology: Groundwater hydrology for engineers*. Academic Press, Orlando, Florida, 1986.

[17] Dershowitz, W. S., and Herda, H. H. Interpretation of fracture spacing and intensity. In *Rock Mechanics*. American Rock Mechanics Association, Santa Fe, New Mexico, 1992, pp. 757–766. doi: 10.1016/0148-9062(93)91769-F.

[18] Emerick, A. A., and Reynolds, A. C. Ensemble smoother with multiple data assimilation. *Computers & Geosciences 55* (2013), 3–15. doi: 10.1016/j.cageo.2012.03.011.

[19] Eshelby, J. D. The Determination of the Elastic Field of an Ellipsoidal Inclusion, and Related Problems. *Proceedings of the Royal Society A: Mathematical, Physical and Engineering Sciences 241*, 1226 (1957), 376–396. doi: 10.1098/rspa.1957.0133.

[20] Fernø, M. A. *A Study of Capillary Pressure and Capillary Continuity in Fractured Rocks*. PhD thesis, University of Bergen, 2008.

[21] Fisher, R. Dispersion on a Sphere. *Proceedings of the Royal Society A: Mathematical, Physical and Engineering Sciences 217*, 1130 (1953), 295–305. doi: 10.1098/rspa.1953.0064.

[22] Floris, F. J. T., Bush, M. D., Cuypers, M., Roggero, F., and Syversveen, A.-R. Methods for quantifying the uncertainty of production forecasts: a comparative study. *Petroleum Geoscience 7* (2001), S87–S96. doi: 10.1144/petgeo.7.S.S87.

[23] Fokker, P. General anisotropic effective medium theory for the effective permeability of heterogeneous reservoirs. *Transport in porous media 44*, 2 (2001), 205–218. doi: 10.1023/A:1010770623874.

[24] Fossen, H., Schultz, R., Shipton, Z., and Mair, K. Deformation bands in sandstone: a review. *Journal of the Geological Society 164*, 4 (2007), 755–769. doi: 10.1144/0016-76492006-036.

[25] Fossum, K. *Assessment of Sequential and Simultaneous Ensemble-based History Matching Methods for Weakly Non-linear Problems*. PhD thesis, The University of Bergen, 2015.

[26] Fukushima, T. Precise and fast computation of the general complete elliptic integral of the second kind. *Mathematics of Computation 80*, 275 (2011), 1725–1725. doi: 10.1090/S0025-5718-2011-02455-5.

[27] Gérard, A., Genter, A., Kohl, T., Lutz, P., Rose, P., and Rummel, F. The deep EGS (Enhanced Geothermal System) project at Soultz-sous-Forêts (Alsace, France). *Geothermics 35*, 5-6 (2006), 473–483. doi: 10.1016/j.geothermics.2006.12.001.

[28] Golf-Racht, T. D. V. *Fundamentals of Fractured Reservoir Engineering*. Elsevier Publishing Company, 1982.

[29] Groshong, R. H. *3-D structural geology: A practical guide to quantitative surface and subsurface map interpretation*. Springer Berlin Heidelberg, 2006. doi: 10.1007/978-3-540-31055-6.

[30] Gudmundsson, A., Marinoni, L. B., and Marti, J. Injection and arrest of dykes: Implications for volcanic hazards. *Journal of Volcanology and Geothermal Research 88*, 1-2 (1999), 1–13. doi: 10.1016/S0377-0273(98)00107-3.

[31] Guéguen, Y., Chelidze, T., and Le Ravalec, M. Microstructures, percolation thresholds, and rock physical properties. *Tectonophysics 279*, 1-4 (1997), 23–35. doi: 10.1016/S0040-1951(97)00132-7.

[32] Gueguen, Y., and Dienes, J. Transport properties of rocks from statistics and percolation. *Mathematical Geology 21*, 1 (1989), 1–13. doi: 10.1007/BF00897237.

[33] Hestir, K., and Long, J. C. S. Analytical expressions for the permeability of random two-dimensional Poisson fracture networks based on regular lattice percolation and equivalent media theories. *Journal of Geophysical Research 95*, B13 (1990), 21565–21581. doi: 10.1029/JB095iB13p21565.

[34] Horne, R. N. *Modern Well Test Analysis: A Computer-Aided Approach*. Petroway, Inc., Palo Alto, 1995.

[35] Huseby, O., Thovert, J.-F., and Adler, P. M. Geometry and topology of fracture systems. *Journal of Physics A: Mathematical and General 30*, 5 (1999), 1415–1444. doi: 10.1088/0305-4470/30/5/012.

[36] Jakobsen, M. Effective hydraulic properties of fractured reservoirs and composite porous media. *Journal of Seismic Exploration 16*, 2-4 (2007), 199–224.

[37] Jakobsen, M., Hudson, J. a., and Johansen, T. A. T -matrix approach to shale acoustics. *Geophysical Journal International 154*, 2 (2003), 533–558. doi: 10.1046/j.1365-246X.2003.01977.x.

[38] Kaufman, A., and Anderson, B. *Principles of Electric Methods in Surface and Borehole Geophysics*, vol. 44. Elsevier B.V., 2010. doi: 10.1016/S0076-6895(10)44007-X.

[39] Kaviany, M. *Principles of Heat Transfer in Porous Media*. Springer New York, 1995. doi: 10.1007/978-1-4612-4254-3.

[40] Kazemi, H., Merrill, L., Porterfield, K., and Zeman, P. Numerical Simulation of Water-Oil Flow in Naturally Fractured Reservoirs. *Society of Petroleum Engineers Journal 16*, 6 (1976), 317–326. doi: 10.2118/5719-PA.

[41] Landau, L. D., and Lifshitz, E. M. *Electrodynamics of continuous media*. Pergamon Press, 1960.

[42] Laubach, S. E. Practical approaches to identifying sealed and open fractures. *AAPG Bulletin 87*, 4 (2003), 561–579. doi: 10.1306/11060201106.

[43] Lee, C.-H., and Farmer, I. *Fluid flow in discontinuous rocks*. Chapman & Hall, London, 1993.

[44] Matthäi, S. K., and Nick, H. M. Upscaling two-phase flow in naturally fractured reservoirs. *AAPG Bulletin 93*, 11 (2009), 1621–1632. doi: 10.1306/08030909085.

[45] Maxwell, J. *A Treatise on Electricity and Magnetism*, vol. 1. Cambridge University Press, 1873. doi: 10.1017/CBO9780511709333.

[46] Milton, G. W. The coherent potential approximation is a realizable effective medium scheme. *Communications in Mathematical Physics 99*, 4 (1985), 463–500. doi: 10.1007/BF01215906.

[47] Milton, G. W. *The Theory of Composites*. Cambridge University Press, Cambridge, 2002. doi: 10.1017/CBO9780511613357.

[48] Mourzenko, V., Thovert, J.-F., and Adler, P. Macroscopic permeability of three-dimensional fracture networks with power-law size distribution. *Physical Review E 69*, 6 (2004), 066307. doi: 10.1103/PhysRevE.69.066307.

[49] Mourzenko, V., Thovert, J.-F., and Adler, P. Percolation of three-dimensional fracture networks with power-law size distribution. *Physical Review E 72*, 3 (2005), 036103. doi: 10.1103/PhysRevE.72.036103.

[50] Mourzenko, V. V., Thovert, J.-F., and Adler, P. M. Permeability of isotropic and anisotropic fracture networks, from the percolation threshold to very large densities. *Physical Review E 84*, 3 (2011), 036307. doi: 10.1103/PhysRevE.84.036307.

[51] Mourzenko, V. V., Thovert, J.-F., and Adler, P. M. Trace analysis for fracture networks with anisotropic orientations and heterogeneous distributions. *Physical Review E 83*, 3 (2011), 031104. doi: 10.1103/PhysRevE.83.031104.

[52] Oda, M. Permeability tensor for discontinuous rock masses. *Géotechnique 35*, 4 (1985), 483–495. doi: 10.1680/geot.1985.35.4.483.

[53] Oliver, D. S., Reynolds, A. C., and Liu, N. *Inverse Theory for Petroleum Reservoir Characterization and History Matching*. Cambridge University Press, 2008. doi: 10.1017/CBO9780511535642.

[54] Persoff, P., and Pruess, K. Two-phase flow visualization and relative permeability measurement in natural rough-walled rock fractures. *Water Resources Research 31*, 5 (1995), 1175–1186. doi: 10.1029/95WR00171.

[55] Pinder, G. F., and Gray, W. G. *Essentials of Multiphase Flow in Porous Media*. Wiley, Hoboken, NJ, 2008.

[56] Pozdniakov, S., and Tsang, C.-F. A self-consistent approach for calculating the effective hydraulic conductivity of a binary, heterogeneous medium. *Water Resources Research 40*, 5 (2004), W05105. doi: 10.1029/2003WR002617.

[57] Rangel-German, E. R., and Kovscek, A. R. Time-dependent matrix-fracture shape factors for partially and completely immersed fractures. *Journal of Petroleum Science and Engineering 54*, 3-4 (2006), 149–163. doi: 10.1016/j.petrol.2006.08.004.

[58] Renshaw, C. E. On the relationship between mechanical and hydraulic apertures in rough-walled fractures. *Journal of Geophysical Research 100*, B12 (1995), 24629. doi: 10.1029/95JB02159.

[59] Sahimi, M. Flow phenomena in rocks: From continuum models to fractals, percolation, cellular automata, and simulated annealing. *Reviews of Modern Physics 65*, 4 (1993), 1393–1534. doi: 10.1103/RevModPhys.65.1393.

[60] Sandve, T. H. *Multiscale simulation of flow and heat transport in fractured geothermal reservoirs*. PhD thesis, University of Bergen, 2013.

[61] Sandve, T. H., Berre, I., and Nordbotten, J. M. An efficient multi-point flux approximation method for Discrete Fracture-Matrix simulations. *Journal of Computational Physics 231*, 9 (2012), 3784–3800. doi: 10.1016/j.jcp.2012.01.023.

[62] Shahraini, A., Ali, A., and Jakobsen, M. Characterization of fractured reservoirs using a consistent stiffness-permeability model: focus on the effects of fracture aperture. *Geophysical Prospecting 59*, 3 (2011), 492–505. doi: 10.1111/j.1365-2478.2010.00934.x.

[63] Sheng, X. Q., and Song, W. *Essentials of Computational Electromagnetics*. John Wiley & Sons, Hoboken, 2012. doi: 10.1002/9780470829646.

[64] Singhal, B. B. S., and Gupta, R. P. *Applied hydrogeology of fractured rocks: Second edition*. Springer Netherlands, 2010. doi: 10.1007/978-90-481-8799-7.

[65] Skjervheim, J.-A., and Evensen, G. An Ensemble Smoother for Assisted History Matching. In *SPE Reservoir Simulation Symposium* (2011), Society of Petroleum Engineers. doi: 10.2118/141929-MS.

[66] Snow, D. T. Anisotropic Permeability of Fractured Media. *Water Resources Research 5*, 6 (1969), 1273–1289. doi: 10.1029/WR005i006p01273.

[67] Terzaghi, R. D. Sources of Error in Joint Surveys. *Géotechnique 15*, 3 (1965), 287–304. doi: 10.1680/geot.1965.15.3.287.

[68] Torquato, S. *Random Heterogeneous Materials*, vol. 16 of *Interdisciplinary Applied Mathematics*. Springer New York, 2002. doi: 10.1007/978-1-4757-6355-3.

[69] van Lingen, P., Daniel, J.-M., Cosentino, L., and Sengul, M. Single Medium Simulation of Reservoirs with Conductive Faults and Fractures. In *11th SPE Middle East Oil Show* (Bahrain, 2001), Society of Petroleum Engineers, pp. 541–547. doi: 10.2523/68165-MS.

[70] Wang, Y., Li, G., and Reynolds, A. Estimation of Depths of Fluid Contacts by History Matching Using Iterative Ensemble-Kalman Smoothers. *SPE Journal 15*, 2 (2010), 509–525. doi: 10.2118/119056-PA.

[71] Warren, J., and Root, P. The Behavior of Naturally Fractured Reservoirs. *Society of Petroleum Engineers Journal 3*, 3 (1963), 245–255. doi: 10.2118/426-PA.

[72] Wen, X.-H., and Gómez-Hernández, J. Upscaling hydraulic conductivities in heterogeneous media: An overview. *Journal of Hydrology 183*, 1-2 (1996), ix–xxxii. doi: 10.1016/S0022-1694(96)80030-8.

[73] Whitaker, S. Advances in Theory of Fluid Motion in Porous Media. *Industrial & Engineering Chemistry 61*, 12 (1969), 14–28. doi: 10.1021/ie50720a004.

[74] Wilt, M. J. Crosswell electromagnetic tomography: System design considerations and field results. *Geophysics 60*, 3 (1995), 871. doi: 10.1190/1.1443823.

[75] Yi, Y., and Tawerghi, E. Geometric percolation thresholds of interpenetrating plates in three-dimensional space. *Physical Review E 79*, 4 (2009), 1–6. doi: 10.1103/PhysRevE.79.041134.

[76] Yi, Y. B., and Esmail, K. Computational measurement of void percolation thresholds of oblate particles and thin plate composites. *Journal of Applied Physics 111*, 12 (2012), 124903. doi: 10.1063/1.4730333.

[77] Zimmerman, R. W., and Yeo, I. Fluid Flow in Rock Fractures: From the Navier-Stokes Equations to the Cubic Law. In *Dynamics of fluids in fractured rock*, B. Faybishenko, P. A. Witherspoon, and S. M. Benson, Eds. American Geophysical Union, 2000. doi: 10.1029/GM122p0213.